A Novel Approach for Surface Topography Simulation Considering the Elastic-Plastic Deformation of a Material During a High-precision Grinding Process

Huiqun Chen[1] and Fenpin Jin[2](✉)

[1] Faculty of Public Curriculum, Shenzhen Institute of Information Technology, 2188 Longxiang Avenue, Shenzhen, China
[2] Bao'an Maternal and Child Health Hospital, 56 Yulv Road, Shenzhen, China
chqleo@163.com

Abstract. A novel simulation approach for 3D surface topography that considers the elastic-plastic deformation of workpiece material during a high-precision grinding process is presented in this paper. First, according to the kinematics analysis for the abrasive grain during the grinding process, the motion trajectory of the abrasive grain can be calculated. Second, the kinematic interaction between the workpiece and the abrasive grains can be established, which integrates the elastic-plastic deformation effect on the workpiece material with the topography, the simulation results are more realistic, and the simulation precision is much higher. Finally, based on an improved surface applied to the grinding wheel, the surface topography of the workpiece is formed by continuously iterating overall motion trajectories from all active abrasive-grains in the process of high-precision grinding. Both the surface topography and the simulated roughness value of this work are found to agree well with those obtained in the experiment. Based on the novel simulation method in this paper, a brand-new approach to predict the quality of the grinding surface by providing machining parameters, selecting effective machining parameters, and further optimizing parameters for the actual plane grinding process, is provided.

Keywords: Surface topography · High-precision grinding · Abrasive grain · Elastic-plastic deformation · Simulation

1 Introduction

There are two important factors affecting the surface quality of the machined workpiece during the high-precision grinding: the abrasive grains (grinding tools) and the debris formation process. In a traditional grinding process, the machining dimension of the parts and the 3D model of the machined surface are obtained by instrument detection after grinding [1–3]. If the processing parameters are selected improperly, the parts will

© The Author(s) 2022
Z. Qian et al. (Eds.): WCNA 2021, LNEE 942, pp. 1176–1193, 2022.
https://doi.org/10.1007/978-981-19-2456-9_118

not meet the technical requirements, which will result in wasting money and resources [4].

With the development of computer technology, the 3D surface of machined parts has been digitally simulated with the help of computers, and this process is usually called virtual manufacturing. Virtual manufacturing is one of the main development directions of modern manufacturing [5–7].

Many researchers have made significant attempts to study the generation mechanism of workpiece surface during grinding process. Malkin [8] described motion trajectory of any abrasive grain and investigated the relationship between the chip thickness and the grinding parameters. A mathematical model to describe the kinematics of the dressed wheel topography and to reflect the ground workpiece surface texture was established by Liu and his co-authors [9]. Kunz and his co-author [10] utilized a machine vision method to survey the wheel topography of a diamond micro-grinding wheel. Nguyen et al. [11] proposed a kinematic simulation model for the grinding operation, in which the complex interaction relationship between the wheel and the workpiece was taken into account during the creation process of the machined surface. The surface topography of the grinding wheel can affect the surface integrity of grinding workpiece. Chen and his co-authors [12] focused on the modeling for grinding workpiece surface founded on the real grinding-wheel surface topography. Cao and his co-authors [13] investigated the influences of the grinding parameters and the grinding mechanism on surface topography of the workpiece, and a novel topography simulation model considered the relative vibration between the grinding-wheel and the workpiece was proposed, concurrently, the wheel working surface topography was taken into account in this model. Nguyen and Butler [14] described a numerical procedure according to a random field transformation for effectively generating the grinding wheel topography. The correlation between the grinding wheel surface topography and its performance was investigated by Nguyen and Butler in another study [15], which was characterized by using 3D surface characterisation parameters. Li and Rong [16] established the micro interference model of single abrasive grain taking the shape and the size properties of the abrasive grain accompanying the crush between the binder and the grain into account. Because of self-excited vibration, surface grinding processes are bound to be chatter. Sun et al. [17] developed a dynamic model with time-delay and two degrees of freedom feature to reveal the correlation of the dynamic system characteristic and the workpiece topography. Liu and his co-authors [18] took the gear grinding as the research object and revealed the chatter effect on the machined surface topography. The grinding operations under different machining states and surface topographies of gears in each process were discussed comprehensively. Jiang et al. [19] established the kinematics model of machining surface topography of workpiece taking the factors of grinding parameters and vibrational features into account.

However, the machined workpiece materials in the above literatures were assumed that they were non-deformed (under ideal conditions), and all of these researches did not take the influence of workpiece material's elastic-plastic deformation on workpiece surface into account. The simulating precision of the above discussed studies lags behind that of the actual machined surface. How to synthetically consider workpiece material's

elastic-plastic deformation during the grinding process and the kinematic prediction for the grinding process proves to be our research emphasis.

In this paper, the abrasive-grain motion trajectory of a plane grinding process is analysed and studied. First, the trajectory equations of abrasive-grain are proposed based on the grinding kinematics. Second, the kinematic interaction relationship between the machining workpiece and the abrasive-grains can be established, a novel approach for surface topography simulation taking the elastic-plastic deformation of a material during a grinding process into account is also developed. Finally, based on the an improved Gaussian surface applied to the grinding wheel, the workpiece surface topography can be formed by continuously iterating overall motion trajectories from all active abrasive-grains in the process of high-precision grinding, and the MATLAB programming method is used to simulate and predict the 3D grinding surface of workpiece.

2 Grinding Kinematics

In the high-precision grinding process, there are two movements: the rotation of the grinding-wheel and the translational movement of the machining workpiece [20, 21].

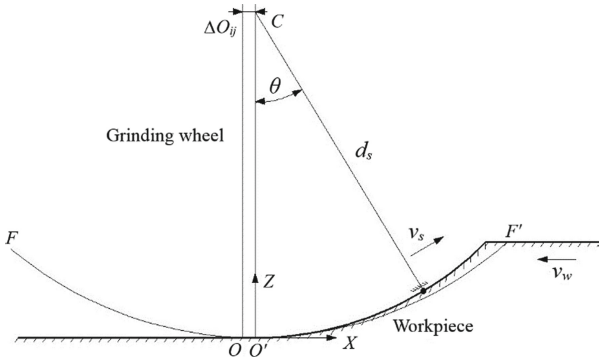

Fig. 1. The motion trajectory of a working abrasive-grain.

In Fig. 1, the coordinates system $O'XYZ$ can be established following the rules that its origin point O' is fixed on the workpiece and coinciding with the abrasive-grain at the lowest point position, and the machining trochoid path $FO'F'$ is formed on the surface of workpiece. This trochoid is synthesized with two motions: abrasive grain rotating around the wheel centre and workpiece translation [11]. The mathematical description of this trochoid is given by Eqs. (1) and (2) [22]:

$$x = \frac{d_s}{2}\sin\theta \pm \frac{d_s v_w}{2v_s}\theta \tag{1}$$

$$z = d_s(1 - \cos\theta) \tag{2}$$

where x and z are the trajectory coordinates of the abrasive-grain, v_w represents the workpiece movement velocity, v_s represents the linear velocity of the grinding-wheel,

θ represents the rotation angle of the grinding-wheel, due to the small of angle θ here, $sin\theta \approx \theta$, and d_s represents the nominal diameter of the grinding-wheel.

t represents the time required for the abrasive-grain rotating counter-clockwise with an angle θ from the lowest position point O', and $t = \frac{d_s\theta}{2v_s}$. The process in which the linear velocity direction of an abrasive grain revolving around the wheel axis is opposite to that of the workpiece movement is referred to as up-grinding, and the symbol $\pm$ is replaced by $+$ in Eq. (1). Otherwise, when down-grinding occurs, $\pm$ is replaced by $-$.

Because θ is very small here, $sin\theta \approx \theta$, the trochoid can be simplified to a parabola:

$$z = \frac{x^2}{d_s\left(1 \pm \frac{v_w}{v_s}\right)^2} \tag{3}$$

Due to the workpiece translation, when abrasive-grains cut the workpiece surface, the coordinate origin of each cutting parabola on the workpiece is different. The distance value ΔO_{ij} from the coordinate origin to the initial cutting position can be expressed as

$$\Delta \mathrm{O_{ij}} = \frac{\Delta \mathrm{L_{ij}} \mathrm{v_w}}{\mathrm{v_s}} \tag{4}$$

where ΔL_{ij} is the arc length that the initial position of the abrasive grain turns, $\Delta L_{ij} = \pi(n-1)\Delta d_s + l_{ij}$, l_{ij} represents the arc length from the grain on the grinding-wheel surface to the initial point, and n represents the rotation cycle of the grinding-wheel.

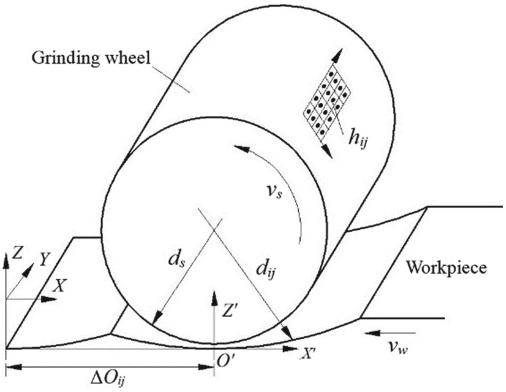

Fig. 2. Cutting model of a single abrasive-grain on a grinding-wheel.

Taking the coordinate system translation and the distance from the abrasive grain to the wheel-axis into account (in Fig. 2), thus the trajectory equation of a single abrasive-grain acting on a grinding wheel surface can be obtained again:

$$\mathrm{z} = \frac{\left(\mathrm{x} - \Delta \mathrm{O_{ij}}\right)^2}{\mathrm{d_{ij}}\left(1 \pm \frac{\mathrm{v_w}}{\mathrm{v_s}}\right)^2} + \mathrm{h_{max}} - \mathrm{h_{ij}} \tag{5}$$

where d_{ij} represents the actual distance from the wheel centre to the top point among the cutting points, $d_{ij} = d_s + h_{ij}$, h_{max} represents the maximum coordinate value among cutting points for all abrasive-grains, $h_{max} = max\{h_{ij}\}$, and h_{ij} is the actual radial height of grain cutting points on the wheel surface.

3 Interaction Mechanism of Abrasive-Grains and Workpiece Material in the Grinding Contact Zone

The force acting on a single abrasive grain normal is regarded similar to the stress condition when testing the Brinell-hardness [23]. The deformation condition can be confined as an elastic-plastic deformation. When the spherical grain moves horizontally (along the direction of linear velocity), the plastic-deformation region on the sphere begins tilting, and the material of grinding workpiece is stacked up and torn from the surface of workpiece to generate debris [24].

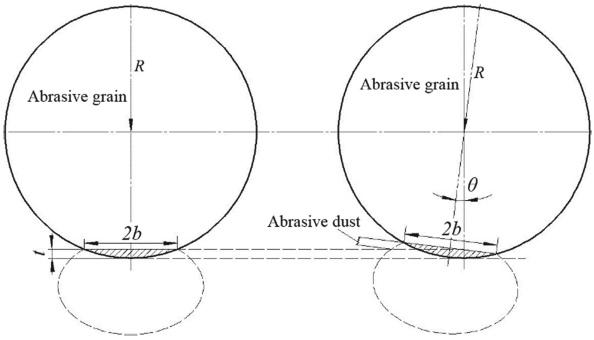

Fig. 3. Action process of a spherical abrasive grain during grinding.

This process is shown in Fig. 3. Where the force R of a single abrasive-grain is derived using the test method of Brinell hardness.

$$\mathrm{R} = \frac{\pi}{3}\mathrm{b}^2\mathrm{HC}' \tag{6}$$

In the contact zone, C' represents the ratio (the mean pressure is divided by the axial stress), where, generally, $C' = 3$, b is equal to half of the grinded workpiece width, H is the Brinell hardness of the workpiece material, and R represents the normal force acting on abrasive-grain.

The grinding-wheel is a porous body that is composed of abrasive-grains, binder, and pores. The abrasive-grains are elastically supported with the binder. During the actual grinding process, due to the movement of the abrasive-grain centre under the cutting force action, it directly causes the actual interference/contact curve between the wheel and the workpiece to be higher than the theoretical one. Meanwhile, the workpiece surface will attain elastic-recovery when finish grinding, therefore, the final curve formed

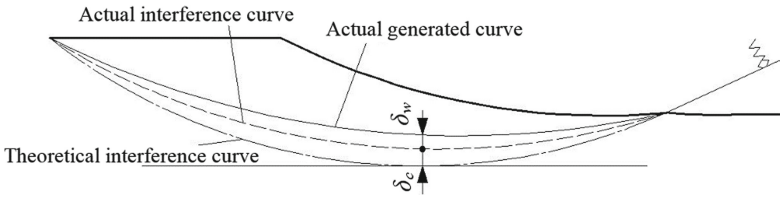

Fig. 4. Action curve of the abrasive-grain.

by the surface formation is higher than the actual interference/contact curve between the grinding-wheel and the machining workpiece (in Fig. 4).

The actual forming curve is realized by attaching the change δ_c of the grain centre, and the elastic-recovery δ_w of the grinding material to the basis of the theoretical interference curve. After discretizing the workpiece surface, the coordinate matrix Z_i^n can be obtained as Eq. (7):

$$\mathrm{Z_i^n} = \min\left(\mathrm{z_i^n} + \delta_{\mathrm{ci}} + \delta_{\mathrm{wi}}, \mathrm{Z_i^{n-1}}\right) \tag{7}$$

where Z_i^n represents the coordinate matrix of workpiece surface when finish cutting of the $n-th$ abrasive-grain, z_i^n represents the theoretical coordinate matrix of the workpiece surface after machining of the *n-th* abrasive-grain, Z_i^{n-1} means the coordinate matrix of workpiece surface after machining of the $(n-1)$-th abrasive-grain, and δ_{ci}, δ_{wi} are two types of deformation values at point i, and their expressions are as follows:

$$\delta_c = C(Rcos\theta)^{2/3} \tag{8}$$

$$\delta_w = Rcos\theta/k \tag{9}$$

where C is a constant value that ranges from 0.08 to 0.25 with an average value of 0.15 [25] and k is the stiffness of the workpiece.

In the grinding process, only the undeformed material is removed by the abrasive-grains, while the remaining unresected material undergoes plastic deformation and is stacked on two sides of abrasive-grains, therefore, the grinding efficiency β is utilized here, which is equal to the ratio of the material volume that is undeformed but removed from workpiece surface to the total volume machined by the abrasive-grain in this zone where the abrasive grain has cut. Then, the area A_p that accumulates on both sides of the abrasive grain due to the plastic deformation can be written as

$$\mathrm{A_p} = \mathrm{A}(1-\beta)/2 \tag{10}$$

The shape of the material that accumulates on both sides of the abrasive grain can be approximated by a parabola (in Fig. 5).

$$z = \frac{(2a-x)xh}{a^2} \tag{11}$$

The workpiece material is stacked on two sides of the orientation of angle α; then, the stacked material area can be obtained from the stacked material curve:

$$A_p = 4ah/3 \tag{12}$$

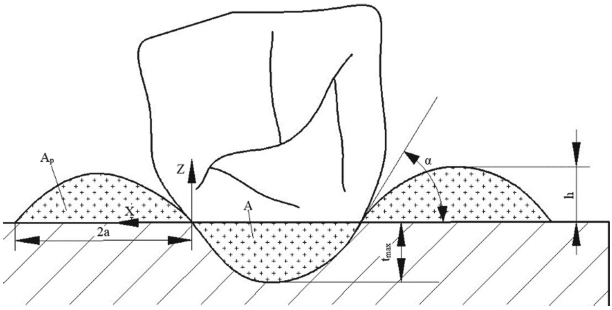

Fig. 5. Plastic accumulation caused by a plough.

Then,

$$a = \sqrt{\frac{3A_p}{2tan\alpha}} \tag{13}$$

$$h = \sqrt{\frac{3A_p tan\alpha}{8}} \tag{14}$$

where $tan\alpha = \frac{t_{max}}{b}$.

4 Simulation of the Workpiece Grinding Surface

During the computer simulation process of the high-precision grinding, such surface parameters of the grinding-wheel can be obtained in two ways. One method is to obtain a height matrix describing the shape of the surface by measuring. This approach, however, takes a lot of time, and computer simulations require massive piece of the wheel-surface. The other method is to randomly generate the position matrix of the abrasive-grains distributed on the grinding-wheel using a computer. Generally, the abrasive-grains are simplified as spheres ignoring the complexity of their shape [26–29]. From a mathematical viewpoint, these abrasive-grains are a set of points with an average distribution in the two-dimensional direction of the wheel surface, and the distances between the grains obey an even distribution [30] in the radial direction. The protrusion-heights of

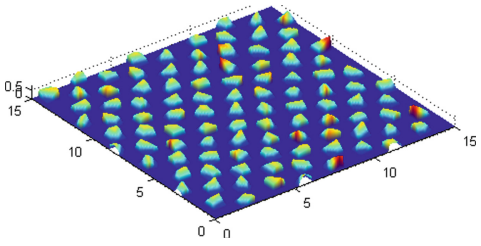

Fig. 6. An improved Gaussian surface of the grinding wheel simulated by the authors of this paper.

these abrasive-grains are described with a distribution [31], furthermore, the size of the abrasive-grain is approximately equal to the number of grains.

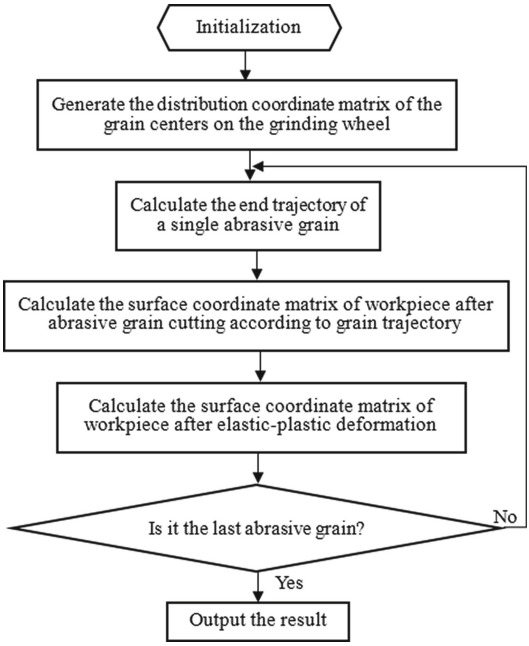

Fig. 7. Computer simulation flow chart.

An improved surface for the grinding-wheel simulated by authors of this paper is shown in Fig. 6. In the computer simulation process, the surface of cutting workpiece can be obtained with the interaction between the abrasive grains and machining workpiece. The trajectory equation of the grain cutting on the workpiece can be obtained from the grinding kinematics model. The machined surface model without elastic-plastic deformation is calculated by the grinding trajectory. The cross sections of the interference formed by the workpiece surface and those abrasive-grains is obtained using the interaction model between the abrasive-grains with the grinding workpiece. The ultimate workpiece surface model is then computed by the cross sectional shapes generated by these interference.

Figure 7 shows the whole simulation process, the flow chart for the axial and circumferential coordinate matrices generation of the abrasive-grain distributed on grinding-wheel surface is shown in Fig. 8. Figure 9 shows the coordinate matrix when finish calculating the elastic-plastic deformation for the workpiece surface.

In the simulation experiment, the material is quenched steel of 45#, and the grinding-wheel is GB70RAP400. The data from the abrasive-grains distributed on the surface of grinding-wheel are as follows: the average gap between two adjacent abrasive-grains in circumferential and axial directions is 0.236 mm, and the variation range is ± 0.15 mm.

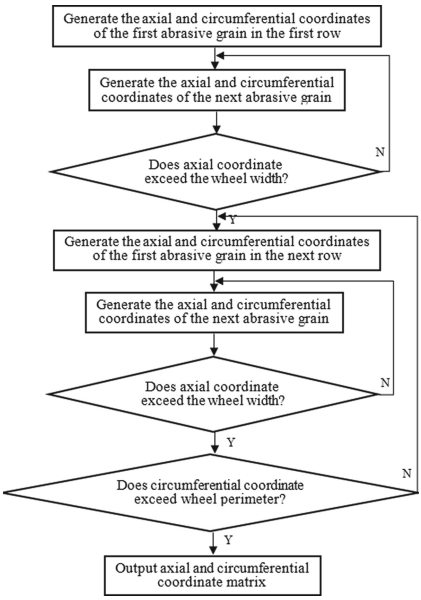

Fig. 8. Flow chart for generating the grain axial deformation of the workpiece material.

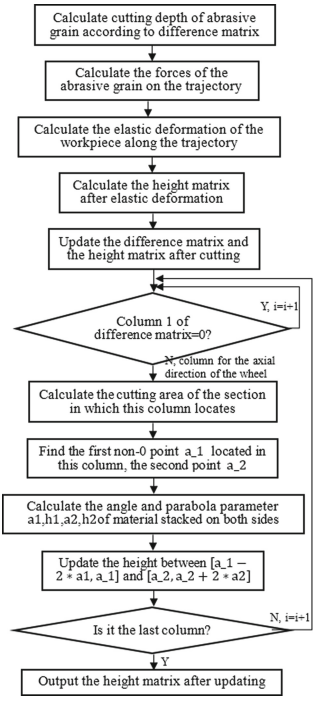

Fig. 9. Flow chart for elastic-plastic and circumferential coordinates.

Table 1. Parametric values of the grinding simulation.

Parameters	Values
Linear velocity of abrasive grains (v_s)	30000 mm/s
Velocity of workpiece translation (v_w)	500/60 mm/s
Nominal diameter of grinding wheel (d_s)	500 mm
Theoretical given cutting depth (a_p)	0.04 mm
Hardness of workpiece material (H)	45HRC (convert to Brinell Hardness when solving)
Coefficient related to the system stiffness of grinding wheel (C)	0.16
Cutting efficiency (β)	0.8
Stiffness of workpiece (k)	320 kg/mm

For these abrasive-grains, the average diameter is 0.125 mm, and the variation range is ±0.11 mm. Table 1 shows the cutting parameters of simulation.

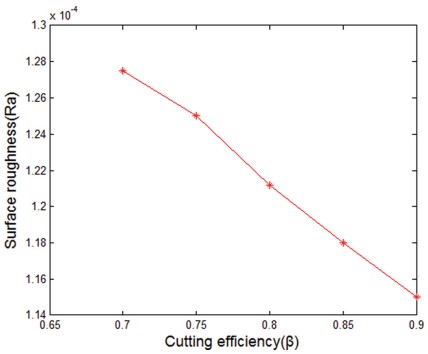

Fig. 10. Relationship between the cutting efficiency and the surface roughness.

When the other parameters are kept unchanged, the surface roughness changes with the cutting efficiency of the workpiece material, which is shown in Fig. 10.

From Fig. 10, a greater cutting efficiency of the workpiece material results in a reduced surface roughness and a better surface quality is obtained, which is the condition under which the other parameters are unchanged. The grinding-wheel surface is meshed (shown in Fig. 11).

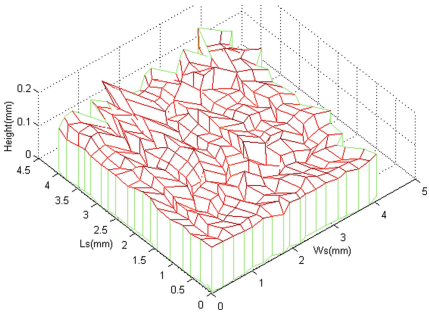

Fig. 11. Simulated wheel topography.

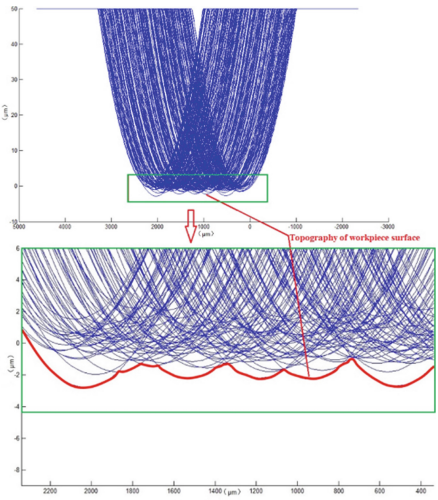

Fig. 12. The workpiece surface topography and the local enlarged drawing.

The workpiece surface topography is formed with continuously iterating the motion trajectories, these motion trajectories are generated by all active abrasive grains in high-precision machining (in Fig. 12). The array of workpiece surface topography needs to be updated

$$\left[G_{ij}\right]^{k} = min\left(\left[G_{ij}\right]^{k-1}, \left[g_{ij}\right]\right) \tag{15}$$

where $\left[g_{ij}\right]$ is defined as the initial array, G_{ij} is the protrusion height array of workpiece surface after cutting, the superscript k represents the surface profile index formed by the *k-th* abrasive-grain. when multi-pass grinding, the preceding simulation for workpiece surface is fed back into the computer program, which is regard as the initial surface texture of the grinding workpiece.

Figure 13 shows a three-dimensional model for the workpiece surface when finish grinding, in which Z represents the height coordinate of the machined workpiece, W_s represents the machined workpiece coordinate in the direction of the grinding-wheel

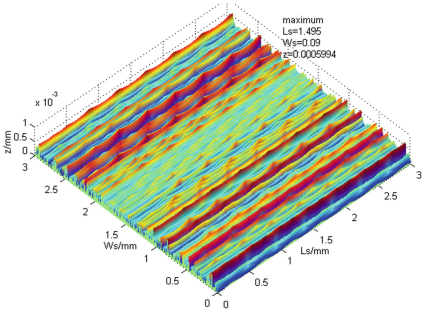

Fig. 13. Simulated surface shape of workpiece.

axis, and L_s is the translational direction coordinate of the workpiece. The labelled values (showing the maximum height and the corresponding position of maximum height) are shown in the upper right corner.

5 Experimental Verification and Analysis

For the sake of verifying the rationality and effectiveness of the algorithm here, comparing the simulation results with the experimental ones is necessary.

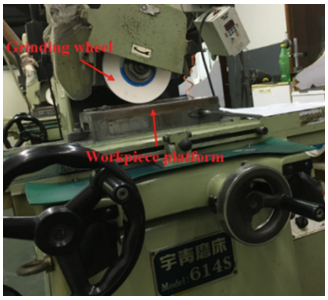

Fig. 14. Yuqing grinder.

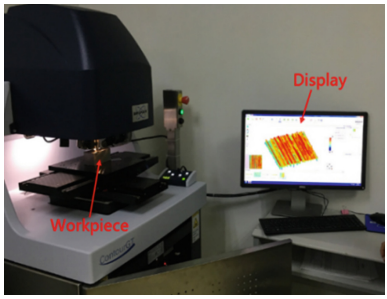

Fig. 15. 3D optical surface profilometer.

Table 2. Roughness values comparison.

Sample no.	Measured roughness R_a (μm)	Simulated roughness R_a (μm)	Error
1	0.272	0.251	7.7%
2	0.344	0.323	6.1%
3	0.305	0.292	4.3%

Three high-precision grinding experiments were implemented on a multi-function grinder (Model 614S, Taiwan Yuqing Company, as shown in Fig. 14). The grinding surface of all machining parameters was investigated with a 3D optical surface profilometer

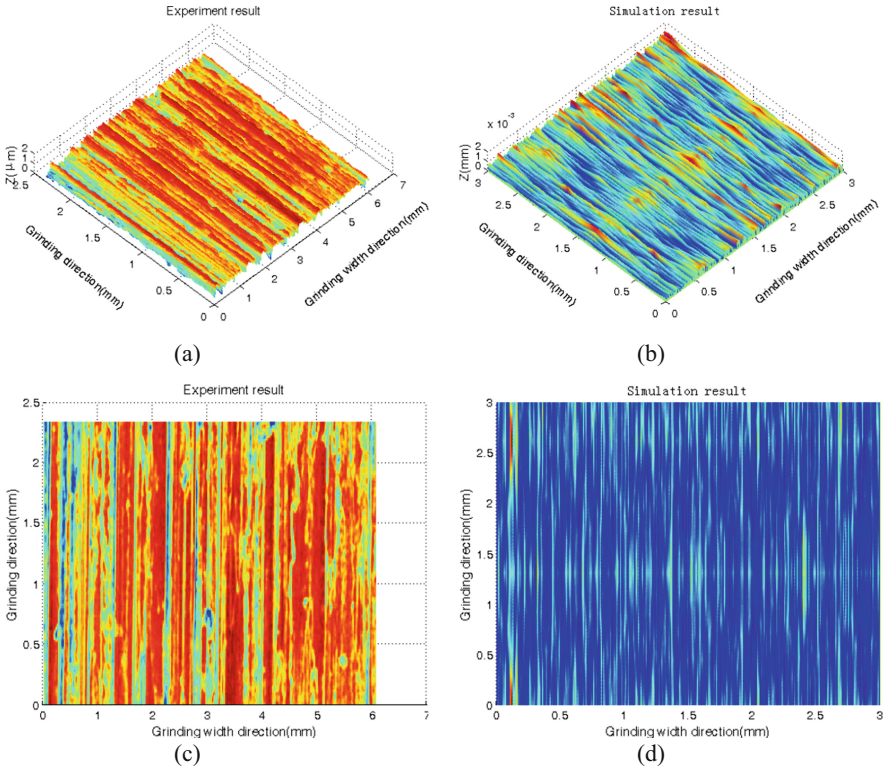

Fig. 16. Comparison of three-dimensional ground surface topography ($v_s = 10$ mm/s, $v_w = 1$ m/min, $a_p = 0.01$ mm)

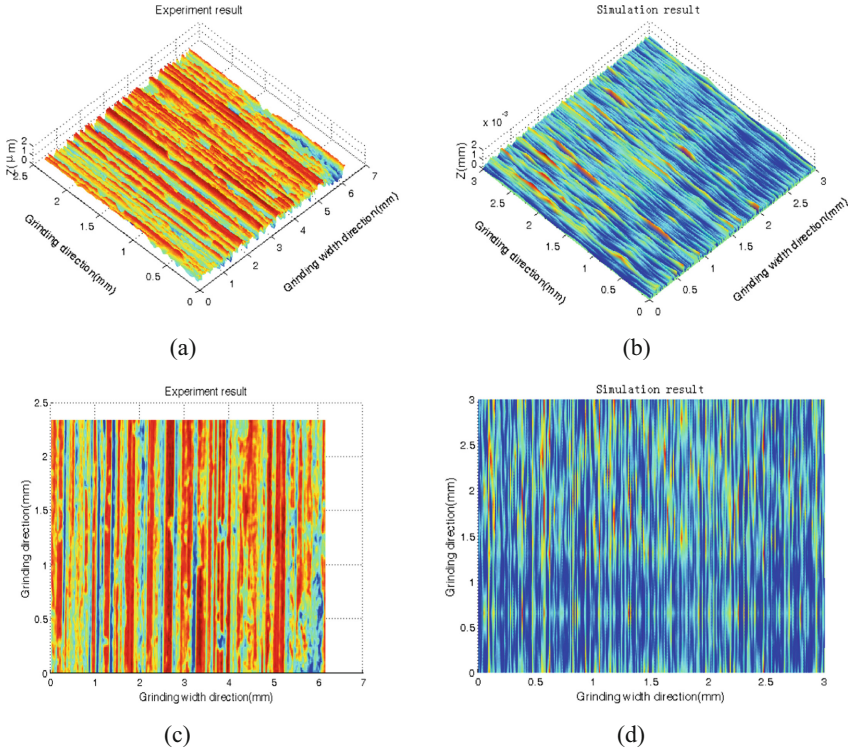

Fig. 17. Comparison of three-dimensional ground surface topography ($v_s = 20$ mm/s, $v_w = 1$ m/min, $a_p = 0.04$ mm).

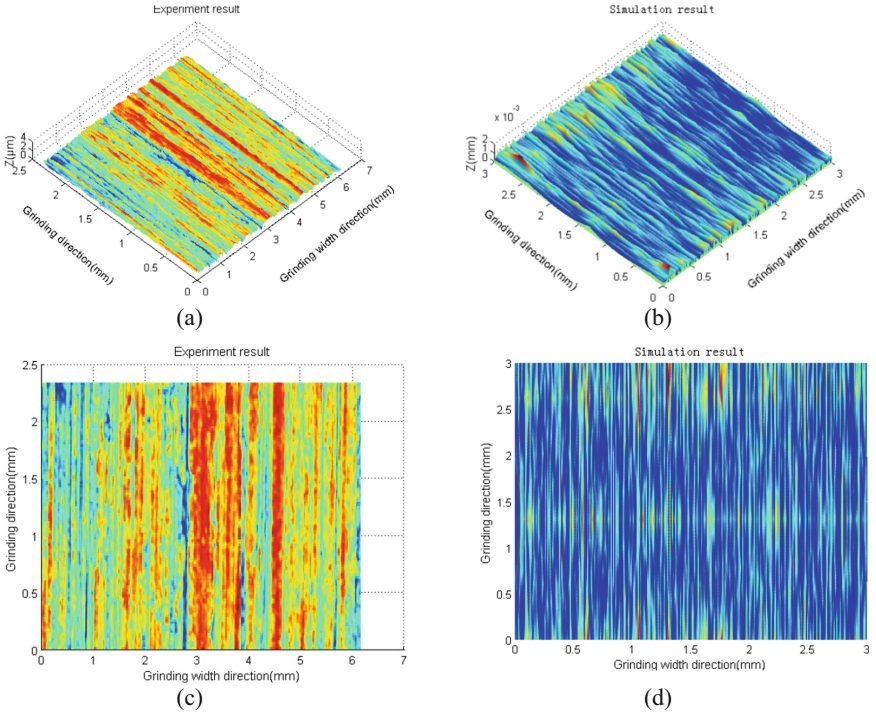

Fig. 18. Comparison of three-dimensional ground surface topography ($v_s = 20$ mm/s, $v_w = 2$ m/min, $a_p = 0.01$ mm).

(ContourGT, American Bruker Company, as shown in Fig. 15). In Figures 16, 17, and 18, the simulated three dimensional surface topography of isometric view figure shown in (b) and top view figure shown in (d), the measured surface topography of isometric view figure shown in (a) and top view figure shown in (c). Table 2 shows that both the measured results and simulation ones have consistent topography features, furthermore, the roughness values also have a small error(less than 8%). In conclusion, it can be said that there is reasonable agreement between the simulated results and the experimental ones.

6 Conclusions

The relationship among the grain parameters, the grinding parameters and the workpiece surface shape is established according to the kinematic model of high-precision grinding and the interaction model between the abrasive-grains and the machined workpiece. The effects of the workpiece material's elastic-plastic deformation are integrated into the kinematic interaction model, the simulation results are more realistic, and the simulation precision is much higher. By using the MATLAB programming environment, based on the an improved Gaussian surface applied to the grinding wheel, the workpiece surface topography can be formed by continuously iterating overall motion trajectories from all

active abrasive-grains in the process of high-precision grinding. When comparing the simulated roughness value and the surface topography of this grinding work, under the same machining conditions, both of them are consistent with the measured workpiece surface. The comparison between the simulations and the measurements shows that the accuracy of the presented model is high enough, and both the measured and simulation results have basically consistent topography features and the roughness values also have a small error which is less than 8%. The 3D surface model of the grinding workpiece can be predicted using a computer simulation test, which can provide a basis for selecting machining parameters and further optimizing the parameters.

Acknowledgements. This work was partially supported by the Guangdong Recognized Scientific Research Project in Colleges and Universities of China (grant number 2020KTSCX299), and the Teaching and Research Program for Guangdong Provincial of China (grant number 2020GXSZ165).

References

1. Godino, L., Pombo, I., Sanchez, J.A., Izquierdo, B.: Characterization of vitrified alumina grinding wheel topography using three dimensional roughness parameters: influence of the crystalline structure of abrasive grains. Int. J. Adv. Manuf. Technol. **113**, 1673–1684 (2021)
2. Kang, M.X., Zhang, L., Tang, W.C.: Study on 3D topography modelling of the grinding wheel with image processing techniques. Int. J. Mech. Sci. **167** (2020)
3. Huang, Y., et al.: Study on the surface topography of the vibration assisted belt grinding of the pump gear. Int. J. Adv. Manuf. Technol. **106**, 719–729 (2020)
4. Stalinskii, D.V., Rudyuk, A.S., Solenyi, V.K.: Topography of surface and sub-surface layers of grinding balls operating in dry and wet grinding models. J. Steel Trans. **51**, 135–143 (2021)
5. Bellalouna, F.: New approach for industrial training using virtual reality technology. Proc. Cirp. **93**, 262–267 (2020)
6. Bellalouna, F.: Industrial case studies for digital transformation of engineering processes using virtual reality technology. Proc. Cirp. **90**, 636–641 (2020)
7. Mohamed, A.-M.O., Warkentin, A., Bauer, R.: Prediction of workpiece surface texture using circumferentially grooved grinding wheels. Int. J. Adv. Manuf. Technol. **89**(1–4), 1149–1160 (2016)
8. Malkin, S.: Grinding Technology: Theory and Applications of Machining with Abrasives. Ellis Horwood, Chichester (1989)
9. Liu, Y.M., Gong, S., Li, J., Cao, J.G.: Effects of dressed wheel topography on the patterned surface texture and grinding force. Int. J. Adv. Manuf. Technol. **93**, 1751–1760 (2017)
10. Kunz, J.A., Mayor, J.R.: Stochastic characteristics in the micro-grinding wheel static topography. J. Micro. Nano. Manuf. **2**, 29–38 (2014)
11. Nguyen, A.T., Butler, D.L.: Simulation of surface grinding process, part II: interaction of abrasive grain with workpiece. Int. J. Mach. Tools Manuf. **45**, 1329–1336 (2005)
12. Chen, C., Tang, J., Chen, H., Zhu, C.C.: Research about modelling of grinding workpiece surface topography based on the real topography of the grinding wheel. Int. J. Adv. Manuf. Technol. **93**, 1–11 (2017)
13. Cao, Y.L., Guan, J.Y., Li, B., Chen, X., Yang, J., Gan, C.: Modelling and simulation of grinding surface topography considering the wheel vibration. Int. J. Adv. Manuf. Technol. **66**, 937–945 (2013)

14. Nguyen, A.T., Butler, D.L.: Simulation of surface grinding process, part I: generation of grinding wheel surface. Int. J. Mach. Tools Manuf. **45**, 1321–1328 (2005)
15. Nguyen, A.T., Butler, D.L.: Correlation of the grinding wheel topography and the grinding performance: a study from a viewpoint of 3D surface characterization. J. Mater. Process Technol. **208**, 14–23 (2008)
16. Li, X., Rong, Y.: Framework of the grinding process modelling and simulation based on the micro-scopic interaction analysis. Robot. Comput. Integr. Manuf. **27**, 471–478 (2011)
17. Sun, C., Niu, Y.J., Liu, Z., Wang, Y.S., Xiu, S.: Study on surface topography considering grinding chatter based on dynamics and reliabilities. Int. J. Adv. Manuf. Technol. **92**, 1–14 (2017)
18. Liu, Y., Wang, X.F., Lin, J., Zhao, W.: Experimental investigation into effect of chatter on the surface microtopography of gears in grinding. J. Mech. Eng. Sci. **231**, 294–308 (2017)
19. Jiang, J.L., Sun, S., Wang, D.X., Yang, Y., Liu, X.: Surface texture formation mechanism based on ultrasonic vibration assisted grinding process. Int. J. Mach. Tools Manuf. **156** (2020)
20. Pan, J.S., Zhang, X., Yan, Q.S., Chen, S.K.: Experimental study of the surface performance of mono-crystalline 6H-SiC substrates in plane-grinding with a metal-bonded diamond wheel. Int. J. Adv. Manuf. Technol. **89**, 619–627 (2017)
21. Priarone, P.C.: Quality conscious optimization of the energy consumption in a grinding process applying sustainability indicators. Int. J. Adv. Manuf. Technol. **86**, 2107–2117 (2016)
22. Uhlmann, E., Koprowski, S., Weingaertner, W., Rolon, D.: Modelling and simulation of grinding processes with mounted points—part 1 of 2-grinding tool surface characterization. Proc. Cirp. **46**, 599–602 (2016)
23. Li, H.N., Yu, T., Wang, Z.X., Zhu, L.D., Wang, W.: Detailed modelling of cutting forces in the grinding process considering variable stages of grain-workpiece micro-interactions. Int. J. Mech. Sci. **126**, 1–45 (2016)
24. Siebrecht, T., et al.: Simulation of grinding processes using FEA and geometric simulation of individual grains. Prod. Eng. **8**, 345–353 (2014)
25. Brinksmeier, E., Heinzel, C., Bleil, N.: Super-finishing and grind strengthening with the elastic bonding system. J. Mater. Process. Technol. **209**, 6117–6123 (2009)
26. Meng, P.: Micro-structure and performance of mono-layer brazed grinding wheel with poly-crystalline diamond grains. Int. J. Adv. Manuf. Technol. **83**, 441–447 (2016)
27. Tahvilian, A.M., Liu, Z., Champliaud, H., Hazel, B., Lagacé, M.: Characterization of the grinding wheel grain topography under different robotic grinding conditions using the confocal microscope. Int. J. Adv. Manuf. Technol. **80**, 1159–1171 (2015)
28. Wang, J.W., Yu, T.Y., Ding, W., Fu, Y., Bastawros, A.: Wear evolution and stress distribution of the single CBN super-abrasive grain in high speed grinding. Precis. Eng. **54**, 70–80 (2018)
29. Zhou, L., Ebina, Y., Wu, K., Shimizu, J., Onuki, T., Ojima, H.: Theoretical analysis on effects of the grain size variation. Precis. Eng. **50**, 27–31 (2017)
30. Palmer, J., Ghadbeigi, H., Novovic, D., Curtis, D.: An experimental study of the effects of dressing parameters on topography of grinding wheels during the roller dressing. J. Manuf. Process. **31**, 348–355 (2018)
31. Xiu, S.C., Sun, C., Duan, J.C., Lan, D.X., Li, Q.L.: Study on surface topography in consideration of dynamic grinding hardening process. Int. J. Adv. Manuf. Technol. **100**, 209–223 (2019)

Open Access This chapter is licensed under the terms of the Creative Commons Attribution 4.0 International License (http://creativecommons.org/licenses/by/4.0/), which permits use, sharing, adaptation, distribution and reproduction in any medium or format, as long as you give appropriate credit to the original author(s) and the source, provide a link to the Creative Commons license and indicate if changes were made.

The images or other third party material in this chapter are included in the chapter's Creative Commons license, unless indicated otherwise in a credit line to the material. If material is not included in the chapter's Creative Commons license and your intended use is not permitted by statutory regulation or exceeds the permitted use, you will need to obtain permission directly from the copyright holder.